for oscillations might give an indication of the mechanism involved.

ACKNOWLEDGMENTS

The authors wish to thank M. Glickman for several very helpful discussions. Special thanks for machining and technical assistance are due to R. W. Yager, H. H. Higgins, and L. Pursell. The crystal face orientation was accomplished by R. T. Smith of RCA Sarnoff Laboratories.

†Work supported jointly by U. S. Atomic Energy Commission under Contract No. AT(30-1)-1238 and by the National Aeronautics and Space Administration.

[1]T. Dodo, Institüt für Plasmaphysik Report No. 2/62, 1967 (unpublished).
[2]K. H. Geissler, Phys. Rev. 171, 179 (1968).
[3]B. J. Eastlund, K. Josephy, R. Leheny, and T. Marshall, Phys. Fluids 9, 2400 (1966).
[4]D. Bohm, E. H. S. Burhop, and H. S. W. Massey, in *Characteristics of Electrical Discharges in Magnetic Fields*, edited by A. Guthrie and R. K. Wakerling (McGraw-Hill, New York, 1949), p. 13.
[5]E. Hinnov and A. S. Bishop, Phys. Fluids 9, 195 (1966).
[6]D. L. Jassby and R. W. Motley, Phys. Fluids 12, 258 (1969).
[7]B. Ancker-Johnson and J. E. Drummond, Phys. Rev. 132, 2372 (1963).
[8]N. J. Harrick, Phys. Rev. 103, 1173 (1954).
[9]B. Ancker-Johnson, in *Proceedings of the International Symposium on Plasma Effects in Solids* (Dunod, Paris, 1964), p. 165.
[10]R. E. Slusher, W. Giriat, and S. R. J. Brueck, Phys. Rev. 183, 758 (1969).
[11]S. W. Kurnick and R. N. Zitter, J. Appl. Phys. 27, 278 (1956).
[12]W. Gartner, Phys. Rev. 105, 823 (1956).
[13]L. L. Campbell, *Galvanomagnetic and Thermomagnetic Effects: The Hall and Allied Phenomena* (Longmans Green, New York, 1923), p. 125.
[14]R. A. Smith, *Semiconductors* (Cambridge U.P., London, 1961), p. 289.
[15]F. J. Morin, Phys. Rev. 93, 62 (1954).
[16]J. Appel and R. Bray, Phys. Rev. 127, 1603 (1962).
[17]D. M. Brown and R. Bray, Phys. Rev. 127, 1593 (1962).
[18]M. A. Habegger and H. Y. Fan, Phys. Rev. Letters 12, 99 (1964).
[19]B. Abeles and S. Meiboom, Phys. Rev. 93, 1121 (1954); 95, 31 (1954).
[20]B. Lax, H. J. Zeiger, R. N. Dexter, and E. S. Rosenblum, Phys. Rev. 93, 1418 (1954).
[21]M. Shibuya, Phys. Rev. 95, 1385 (1954).
[22]H. Y. Fan, *Solid State Physics* (Academic, New York, 1955), Vol. I, p. 283.
[23]H. Jones, Proc. Roy. Soc. (London) A155, 653 (1936).
[24]A. C. Beer, *Solid State Physics* (Academic, New York, 1963), Vol. IV, p. 199.
[25]J. W. McClure, Phys. Rev. 101, 1642 (1956).
[26]C. Goldberg, E. N. Adams, and R. E. Davis, Phys. Rev. 105, 865 (1957).
[27]R. Willardson, T. Harman, and A. Beer, Phys. Rev. 96, 1512 (1954).
[28]J. S. Blakemore, *Semiconductor Statistics* (Pergammon, New York, 1962), p. 282.
[29]H. P. Furth and R. W. Waniek, Phys. Rev. 104, 343 (1956).
[30]CP4A: 25 ml HNO_3, 15 ml HF.
[31]Ge No. 5: 40 ml HF, 6 ml 30% H_2O_2, 24 ml distilled water.
[32]S. G. Ellis, J. Appl. Phys. 28, 1262 (1957).
[33]W. E. Pinson and R. Bray, Phys. Rev. 136, A1449 (1964).
[34]W. Kaiser, R. J. Collins, and H.Y. Fan, Phys. Rev. 91, 1380 (1953).
[35]H. B. Briggs and R. C. Fletcher, Phys. Rev. 91, 1342 (1953).
[36]A. R. Moore and J. O. Kessler, Phys. Rev. 132, 1494 (1963).

PHYSICAL REVIEW A VOLUME 5, NUMBER 1 JANUARY 1972

Photoionization Cross Section of the Neutral Iron Atom*

Hugh P. Kelly and Akiva Ron†
Department of Physics, University of Virginia, Charlottesville, Virginia 22901
(Received 31 March 1971)

Calculations are presented for the photoionization cross section of the neutral iron atom for photon energies from threshold to 10 keV. Our results are based upon the use of nonrelativistic wave functions and the dipole approximation. Correlations are included to low orders by the use of many-body perturbation theory; and the cross section including correlations is found to differ greatly from that obtained from the Hartree-Fock approximation. Hartree-Fock results are also presented for comparison. We roughly estimate our cross section, including correlations near threshold, to be accurate to within a factor of 2 when integrated over a few eV.

I. INTRODUCTION

Photoionization cross sections are of considerable interest in atomic physics and in astrophysics, and it is desirable to have reliable cross sections over a wide range of energy for many elements. Excel-

lent reviews of the photoionization problem have been given recently by Fano and Cooper[1] and by Marr.[2] For the neutral iron atom, there does not seem to be either a measurement or a reasonably accurate calculation of the photoionization cross section. However, this cross section for Fe is of interest at present in astrophysics.[3]

In this paper we present a rather detailed calculation for the photoioniztion cross section for the neutral iron atom in the $(3d)^6\ (4s)^2\ ^5D$ ground state for photon energies ranging from threshold at 7.90 eV to 10 keV. Our calculation is based upon use of the many-body perturbation theory of Brueckner[4] and Goldstone[5] (BG) and use of our techniques[6-8] for applying BG theory to atoms. We have used the dipole approximation and neglected relativistic effects. Our lowest-order result is essentially the Hartree-Fock cross section and our higher-order terms include correlation effects by means of perturbation theory. We have previously calculated the photoionization cross section for Be by BG theory but including only correlations in the ground state.[7] Our methods for applying BG theory to atoms were also used to calculate the photoionization cross section for Li.[9] The present paper is a good illustration of the use of many-body perturbation theory in photoionization calculation.

In obtaining a prescription for applying many-body perturbation theory to the photoionization problem, we use the relation[1]

$$\sigma(\omega) = (4\pi/c)\,\omega\,\mathrm{Im}\alpha(\omega)\ , \tag{1}$$

where $\sigma(\omega)$ is the photoionization cross section, $\alpha(\omega)$ is the frequency-dependent polarizability,[10,11] ω is the photon energy in atomic units, and c is the speed of light (137.036 in a.u.). Atomic units are used throughout this paper unless specified otherwise. Diagrams for $\alpha(\omega)$ have been discussed previously.[10,11] A discussion of many-body methods for the atomic photoeffect has been given by Amusia[12] who with co-workers[13] has carried out successful calculation on the inert gases by means of the random phase approximation. Wendin[14] has discussed the connection between atomic resonances and many-body diagrams.

Section II contains the theory. Section III contains numerical results including the total photoionization cross section and also cross sections for the individual subshells. Hartree-Fock results are given in addition to results containing effects of electron correlations. Correlations are found to affect the calculated cross section very strongly. Section IV contains the discussion and conclusions.

II. THEORY

We consider a perturbing electric field $F\hat{z}\cos\omega t$ so that we have a time-dependent perturbation

$$V_{ex}(\vec{r}, t) = F\cos\omega t \sum_{i=1}^{N} z_i\ , \tag{2}$$

where N is the total number of electrons. The induced dipole moment $\vec{P}$ is given by[11]

$$\vec{P} = \alpha(\omega)\, F\vec{z}\cos\omega t\ , \tag{3}$$

where $\alpha(\omega)$ is the frequency-dependent polarizability. The Hamiltonian is now

$$H = H_0 + H_c' + V_{ex}(\vec{r}, t)\ , \tag{4}$$

where

$$H_0 = \sum_{i=1}^{N} \left[-\tfrac{1}{2}\nabla_i^2 - Z/r_i + V(r_i) \right] \tag{5}$$

and

$$H_c' = \sum_{i<j=1}^{N} r_{ij} - \sum_{i=1}^{N} V(r_i) \tag{6}$$

The single-particle potential $V(r_i)$ is chosen to account for the average interaction of the ith electron with the other $N-1$ electrons.[4,7] The solution of the time-dependent Schrödinger equation with H given by Eq. (4) is[5]

$$\Psi(t) = e^{-iH_0 t}\, U_\alpha(t)\, \Phi_0\ , \tag{7}$$

where Φ_0 is the unperturbed state given by

$$H_0\Phi_0 = E_0\Phi_0 \tag{8}$$

and $U_\alpha(t)$ is the time-evolution operator.[5]

In calculating $\alpha(\omega)$, we use the fact that $-\alpha(\omega)F^2$ is equal to the sum of all (time-independent) energy diagrams, with appropriate denominators shifted by $\pm\omega$, in which there are only two interactions with $F\sum_i z_i$ and any number of interactions with H_c'.[11] Energy denominators between the two interactions with $F\sum_i z_i$ are shifted by $+\omega$ or by $-\omega$, and both types of diagrams contribute to $\alpha(\omega)$. In using perturbation theory we require a complete set of single-particle states which satisfy

$$\left[-\tfrac{1}{2}\nabla^2 - Z/r + V(r) \right] \phi_n = \epsilon_n \phi_n \tag{9}$$

Our unperturbed state Φ_0 is a determinant (or linear combination of determinants) containing N different single-particle states ϕ_n.

The lowest-order contribution to $\alpha(\omega)$ from the state ϕ_p occupied in Φ_0 is given by

$$-\sum_k{}' \left| \langle k | z | p \rangle \right|^2 \left(\frac{1}{\epsilon_p - \epsilon_k - \omega} + \frac{1}{\epsilon_p - \epsilon_k + \omega} \right)\ , \tag{10}$$

where the sum over k includes all excited states, i.e., those not occupied in Ψ_0.

In order to derive Eq. (1), we consider Eq. (10). If we let $|p\rangle$ and $|k\rangle$ now represent exact eigenstates of $H_0 + H_c'$ and z represent $\sum_i z_i$, then Eq. (10) gives $\alpha(\omega)$ exactly. Since $\epsilon_p - \epsilon_k + \omega$ may vanish,

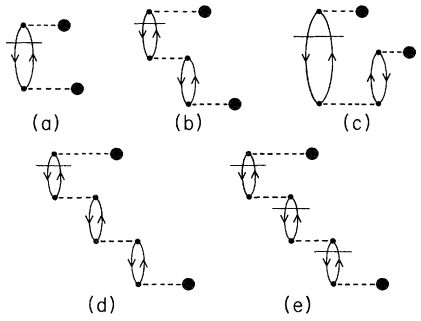

FIG. 1. Diagrams contributing to the photoionization cross section or $\mathrm{Im}\alpha(\omega)$. The horizontal line indicates that the denominator should be treated according to $-i\pi\delta$. The solid dot indicates a matrix element of z.

we add a small imaginary part $i\eta$. We note that

$$\lim_{\eta\to 0}(\epsilon_p-\epsilon_k+\omega+i\eta)^{-1}$$

$$=P(\epsilon_p-\epsilon_k+\omega)^{-1}-i\pi\delta(\epsilon_p-\epsilon_k+\omega), \quad (11)$$

where P represents a principal value integration. We then replace $\sum_k$ by $(2\pi)\int_0^\infty dk$ for continuum states.[6,7] This assumes our continuum states are normalized according to

$$R_k(r)\to\cos[kr+\delta_l+(q/k)\ln 2kr-\tfrac{1}{2}(l+1)\pi]/r \quad (12)$$

as $r\to\infty$, where $V(r)\to q/r$. Inserting Eq. (11) into Eq. (10) and replacing $\sum_k$ by $(2\pi)\int dk$, we find

$$\mathrm{Im}\alpha(\omega)=(2k)\,|\langle k\,|\,z\,|\,p\rangle|^2 \quad , \quad (13)$$

where

$$k=(2\epsilon_p+2\omega)^{1/2} \quad . \quad (14)$$

Substituting Eq. (13) into Eq. (1), we obtain

$$\sigma(\omega)=(8\pi\omega/ck)\,|\langle k\,|\,z\,|\,p\rangle|^2, \quad (15)$$

which agrees with $\sigma(\omega)$ as given, for example, by Bethe and Salpeter[15] when we use atomic units and note that their continuum states are normalized so that asymptotically they are $(2/\pi k)^{1/2}$ times Eq. (12). From now on, states $|p\rangle$ and $|k\rangle$ will again refer to unperturbed solutions of Eq. (9).

In calculating Im $\alpha(\omega)$ we note that only denominators with $+\omega$ contribute. The lowest-order contribution to $\sigma(\omega)$ comes from Eq. (10) and is shown in Fig. 1(a). The heavy dot represents a matrix element of z and the horizontal line indicates the $-i\pi\delta$ contribution from Eq. (11). This notation has been used by Wendin.[14] Every diagram contributing to $\sigma(\omega)$ must have an odd number of horizontal lines. When there is no horizontal line, the denominator is to be treated by a principal value integration.

In the next order of perturbation theory in H_c', we have diagrams with two interactions with z and with one interaction with H_c' as shown in Figs. 1(b) and 1(c). Diagrams 1(b) and 1(c) also occur inverted and with exchange. We also have diagrams like Fig. 1(a) but with an insertion on either the particle or hole line. In the next order in H_c', we have diagrams with two interactions with z and with one interaction with H_c' as shown in Figs. 1(b) and 1(c). Diagrams 1(b) and 1(c) also occur inverted and with exchange. In the next order in H_c', there are diagrams in which the interactions of Fig. 1(b) or 1(c) is repeated as in Fig. 1(d). There are also many new types of diagrams including that of Fig. 1(e) in which three denominators contribute $-i\pi\delta$. Interactions of the types shown are also repeated in still higher orders. There are also many additional new types of diagrams.

In calculating diagrams such as 1(a)–1(d), it is often convenient to consider only that part on either the top or bottom of the horizontal line. We then consider diagrams of the types shown in Fig. 2. For a given p and k, we include many diagrams contributing to $\mathrm{Im}\alpha(\omega)$ by adding the diagrams of Fig. 2 and squaring the sum. We repeat this procedure for different unexcited states p. We may add the effects of diagrams like Fig. 1(e) separately.

When we calculate diagrams such as Fig. 1(b) or Figs. 2(b) and 2(c), there is the possibility of resonances occuring when k' is a bound excited state and $\epsilon_p-\epsilon_k$ equals $\epsilon_q-\epsilon_{k'}$. Higher-order diagrams may be included[11] to shift the position of the resonance from $-\epsilon_q+\epsilon_k'$ and to give it an imaginary part or equivalent width.[14] Shifts in positions of the resonance are contributed by geometrical sums of diagrams like Figs. 1(b) and 1(d). Resonances in diagrams like Figs. 2(b) and 2(c) involve exci-

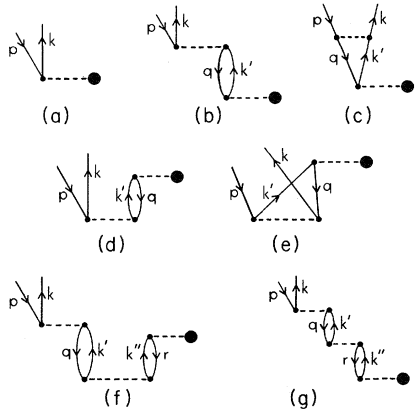

FIG. 2. Open diagrams contributing to the photoionization cross section $\sigma(\omega)$. These represent the bottom parts of diagrams like Fig. 1 after separation by the horizontal line. Diagrams (b)–(e) are first order in the Coulomb interaction H_c'.

tations from state q to a bound excited state k', where ϵ_q is more negative than ϵ_p. In this paper we have resonances in $\sigma(\omega)$ due to $3d \rightarrow np$ excitations degenerate in energy with $4s \rightarrow kp$ excitations, where kp is a continuum state and np is bound.

Many open diagrams which are second order in H_c' are shown in Figs. 3(a)–3(e). Diagrams 3(a), 3(b), 3(d), and 3(e) also contribute to resonances. For example, in Fig. 3(a), the denominator between the two Coulomb interactions is $\epsilon_p + \epsilon_q - \epsilon_k'' - \epsilon_k''' + \omega$, which may vanish for certain bound states ϵ_k'' and ϵ_k''' provided ω is sufficiently large. Inclusion of higher-order diagrams will shift the denominator to a more accurate resonance position.[7,11,14] The diagram of Fig. 3(f) contributes to the width of resonances of Fig. 2(b) by giving an imaginary part to the denominator of Fig. 2(b) after a geometric sum of diagrams like Fig. 3(f) is carried out. Diagrams such as Fig. 3(a) have contributions in Fe, for example, from $(3d)^6(mp)(ns)\,{}^5F$, ${}^5D$, ${}^5P$ states where $m \geq 4$ and $n \geq 5$. In this case, $pq = 4s^{\pm}$ and $k'', k''' = mp, ns$. There are also resonance contributions with mp, ns replaced by md, np with $m, n \geq 4$.

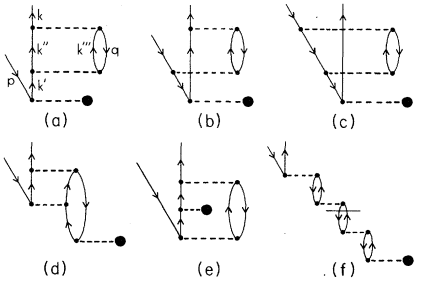

FIG. 3. (a)–(e) Some additional open diagrams second order in H_c'. Diagrams (a), (b), (d), (e), and (f) contribute to resonances in $\sigma(\omega)$. (f) Contribution to the width of resonance in Fig. 2(b).

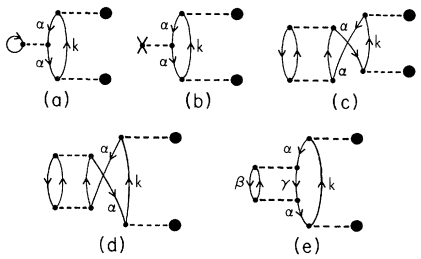

FIG. 4. Diagrams which contribute to shifts in single-particle energies. These should be considered in order to obtain accurate ionization potentials.

III. CALCULATIONS

A. Ionization Energies

In this section we report results for $\sigma(\omega)$ for the ground state of Fe with a configuration $(1s)^2(2s)^2(2p)^6(3s)^2(3p)^6(3d)^6(4s)^2\,{}^5D$. Our single-particle states are those used in a previous calculation[16] of the hyperfine contact term in Fe. All $l = 0$ states were calculated with the Hartree-Fock (HF) $4s$ equation for Fe. The $1s$, $2s$, and $3s$ states are not exactly HF solutions, although the maximum deviation from HF solutions is 0.001 in the radial part of the wave function. Our resulting $2p$ and $3p$ states are close to HF states.[16] The $l = 2$ states were all calculated with the HF $3d$ equation. The $l = 3$ states were calculated in the field of all Fe electrons with one $3d$ electron removed.

In order to have the thresholds for ionization of the various subshells agree as closely with experiment as possible, we made use of experimental ionization potentials from Moore[17] and from Siegbahn *et al.*[18] If we consider the $M_S = +2$ states of Fe $(3d)^6(4s)^2\,{}^5D$, there is a filled half-shell of $3d$ electrons with m_l, m_s values $+2^+, +1^+, 0^+, -1^+, -2^+$; and there is a single $3d$ electron with $m_l = M_L$ and $m_s = -\frac{1}{2}$. The energies of the $4s^-$ and $4s^+$ states differ since the $4s^+$ state has exchange interactions with five $3d$ electrons, whereas $4s^-$ has a single $3d$ exchange interaction. Similarly, we expect the $3d^-$ energy to be different from $3d^+$.

The most important diagrams which shift the ionization potential from the value of the HF single-particle energy are shown in Fig. 4. As discussed previously,[6,11,19] these diagrams may be summed geometrically to shift the HF orbital energy $\epsilon(\alpha)$ to a new value $\epsilon'(\alpha) = \epsilon(\alpha) + \Delta(\alpha)$. For $4s^-$, we find

$$\epsilon'(4s^-) = \epsilon(4s) + 2\langle 4s3d \mid v \mid 3d4s \rangle + \sum_{\alpha \neq 4s^-} E_{\mathrm{corr}}(4s^-, \alpha) + \Delta'(4s') \quad , \quad (16)$$

where $E_{\mathrm{corr}}(4s^-, \alpha)$ is the pair correlation energy of $4s^-$ with α, and $\Delta'(4s^-)$ is the remaining shift due to diagrams like Fig. 4(e). In our calculations ϵ_{4s} is -0.25834 a.u., $2\langle 4s3d \mid v \mid 3d4s \rangle$ is 0.01343 a.u., and $\sum E_{\mathrm{core}}(4s^-, \alpha)$ is -0.07538 a.u.[20] A rough estimate of $\Delta'(4s^-)$ gives $+0.0377$ au., and then $\epsilon'(4s^-)$ is -0.2826 a.u., as compared with the value -0.2903 a.u. for the ionization potential of Fe from Ref. 17. In calculating $\sigma(\omega)$, we have used $\epsilon'(4s^-) = -0.2903$ a.u. We have calculated $\epsilon'(4s^+) - \epsilon'(4s^-)$ as -0.0200 a.u., and so $\epsilon'(4s^+) = -0.3103$ a.u. From Ref. 17, we find $\epsilon'(3d^-) = -0.39648$ a.u. We then calculated an average value for $\epsilon'(3d^+) = -0.5811$ a.u. This value is consistent with the experimental result from Ref. 17 that the $(3d)^5(4s)^2\,{}^4D$ state lies 0.5657 a.u. above the $(3d)^6(4s)^2\,{}^5D$ ground state. Our remaining single-particle energies were obtained from Ref. 18 and are listed in Table I. We used average values for $3p$ and $2p$ rather than distinguish between

TABLE I. Single-particle energies used in calculating $\sigma(\omega)$.

State[a]	Energy[b] (eV)
$4s^-$	7.9004
$4s^+$	8.446
$3d^-$	10.789
$3d^+$	15.813
$3p$	56.003
$3s$	95.006
$2p$	716.543
$2s$	846.051
$1s$	7114.43

[a]These represent single-particle states occupied in the $(3d)^6(4s)^2\,{}^5D$ ($M_S=+2$) ground state of Fe.

[b]Experimental data from Refs. 17 and 18 and also calculations were used to obtain these values.

$j=\frac{3}{2}$ and $\frac{1}{2}$.

B. Photoionization Cross Section

Our lowest-order calculation for $\sigma(\omega)$ is obtained by calculating the diagram of Fig. 1(a) or, equivalently, the diagram of Fig. 2(a) for all states p occupied in our initial determinant. This corresponds closely to a Hartree-Fock calculation of $\sigma(\omega)$ since our single-particle states are either HF solutions or very close to HF solutions. Since the Fe ground state is not spherically symmetric, we average over M_L in calculating $\sigma(\omega)$ or $\sigma(\omega)$.

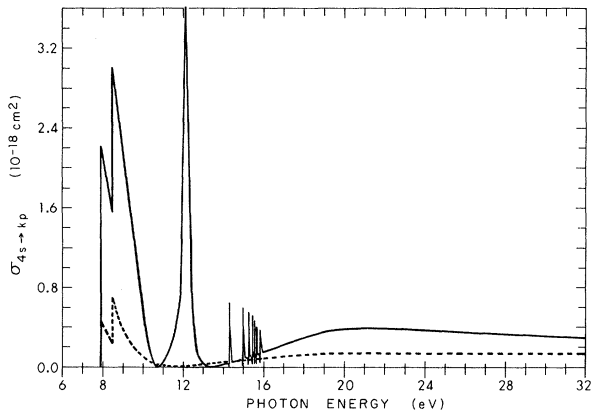

FIG. 5. Contribution to the photoionization cross section from the $(4s)^2$ subshell of Fe. Dashed line: Hartree-Fock or lowest-order result; solid line: includes corrections due to correlations. The resonances shown are due to autoionizing states $(3d)^5(4s)^2\,np\;{}^5P$, ${}^5D$, and ${}^5F$ in which the $(3d)^5$ core couples to ${}^4P$, ${}^4D$, ${}^4F$, or ${}^4G$. In our figure all the contributions with a given np are shown as a single line. However, experiment should show considerable splitting of the line. Our results in the vicinity of the resonances are expected to be inaccurate. Only the lowest-order perturbation contributions are included for resonances. Additional resonances due to $4s^+\to np^+$ excitations and resonances due to $3d^-\to np$ ($n\geq 5$) and $3d^-\to nf$ excitations are also present but are not shown in this figure.

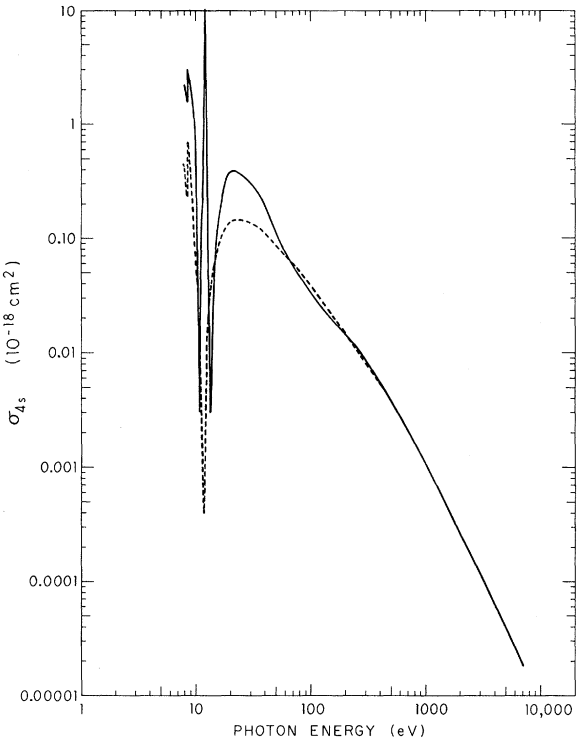

FIG. 6. Contribution to the photoionization cross section from the $(4s)^2$ subshell. Dashed line: Hartree-Fock or lowest-order result; solid line: includes correlation corrections. More detail near threshold is given in Fig. 5.

In this paper we have used L-S coupling and neglected spin-orbit effects which are small.[17] In L-S coupling, $\sigma(\omega)$ is independent of M_S, and we have chosen $M_S=+2$ so that our ground state is a single determinant. This is desirable, though not necessary, in the many-body treatment.

Since we use single-particle energies as listed in Table I, our lowest-order results for $\sigma(\omega)$ differ a little from those obtained using restricted HF solutions. For example, the $4s^-$ and $4s^+$ thresholds do not occur together. Our lowest-order result for the contribution to $\sigma(\omega)$ from the $(4s)^2$ subshell is shown as the dotted line in Figs. 5 and 6. In all figures, the dashed line is the lowest-order result.

Of course, there will be some smearing of the ionization threshold due to fine-structure effects. In the ground state, the fine-structure splitting is 978 cm^{-1} or 0.12 eV from Ref. 17.

We then calculated the contributions to $\sigma(\omega)$ from the diagrams shown in Figs. 2(b)–2(e) and from Figs. 2(f) and 2(g) with $k', k''=4p$. We found very large contributions from the diagram of Fig. 2(b) for $p=4s^+$, $q=4s^-$, and $k'=4p^-$. The dipole matrix

element $\langle 4p \mid z \mid 4s \rangle$ is very large, resulting in the large effect from diagram 2(b). The diagrams of Figs. 2(a), 2(b), and 2(d), for $p = 4s^-$, $q = 4s^+$, and $k = 0.125$ ($\omega = 8.113$ eV) have the respective values -0.1680, -0.4208, and $+0.1215$, with most of the contribution coming from $k' = 4p$. At higher values of k ($k \gtrsim 1.00$), diagram 2(a) becomes the largest. We also included diagrams shown in Figs. 2(f) and 2(g) with $p = r = 4s^{\pm}$, $q = 4s^{\mp}$, $k' = 4p^{\pm}$. Figure 2(g) and higher iterations may be summed geometrically when the hole lines are $4s^+$ and $4s^-$ and particle lines are $4p^{\pm}$. For $k = 0.125$, the effect is to multiply diagram 2(b) by 1.330. The effect decreases with increasing k so that at $k = 1.00$ the factor is 1.070. We also included some of the contributions from Figs. 3 by including the diagrams of Figs. 3(a)–3(d) when one of the excited states is $3d^-$. The contribution from these terms is approximately 5% of the diagrams of Fig. 2. However, a complete calculation of all excited states for these diagrams could yield a significant contribution, particularly from resonances. We also included diagrams like Fig. 1(e) and higher iterations. The maximum contribution came near threshold and reduced $\sigma(\omega)$ by approximately 8%. In calculating diagrams 2(b) –2(g), we did not include all combinations of p and q since there is little correlation between subshells which are far apart.[20] For $p = 4s^{\pm}$, we included $q = 4s^{\mp}$ and $q = 3d^{\pm}$. For $p = 3d^{\pm}$, we included $q = 4s^{\pm}$, $3d^{\pm}$, and $3p^{\pm}$. Contributions with $q = 3p$ were small. Except for resonances, we estimate that contributions for $\sigma(\omega)$ from the $3p$, $3s$, $2p$, $2s$, and $1s$ subshells are given reasonably accurately by the lowest-order (Hartree-Fock) result, and we did not include correlation corrections for them. In these calculation we included all diagrams with one Coulomb interaction as shown in Figs. 1 and 2. Many diagrams with two or more Coulomb interactions were not included so as to make the calculation tractable in a first treatment. However, in future work we plan to include all these diagrams. Since we sum over a complete set of excited single-particle states, we effectively include all configurations in which there is a single excitation but no rearrangement of the angular momentum of the remaining electrons. We only included excitations of the $4s$, $3d$, and $3p$ electrons for the configuration mixing. Since diagrams like Fig. 1(c) and Figs. 2(d), 2(e), and 2(f) were included, we have doubly excited configurations which mix with the ground state. For example, all configurations of the types $(kpk'p)\,^1S$ which mix with $(4s)^2\,^1S$ are included. There are, however, many other configurations which may be quite important but were not considered since we did not calculate many of the diagrams with two or more Coulomb interactions. We omitted the doubly excited configurations which mix with our final state and are present between the two Coulomb interactions shown in Figs. 3(a), 3(b), 3(d), and 3(e). These contributions may be important and contribute to resonances. We did include such configurations for the case where one of the excited states is $3d^-$.

Our results for the $(4s)^2$ subshell are shown in Figs. 5 and 6. The dashed line is the HF result and includes only diagrams 1(a) or 2(a); and the solid line includes the higher-order effects as described. The large difference near threshold between the two curves is almost entirely due to the large contribution from $q = 4s$ and $k' = 4p$ in Fig. 2(b). Since diagrams of Fig. 2 are squared in calculating $\sigma(\omega)$, the effect of 2(b) is even further increased. In the range 7.900–8.446 eV there are excitations $4s^+ \rightarrow np^+$ (for large n) which are degenerate with $4s^- \rightarrow kp^-$ and give rise to resonances. However, the over-all effect from these is weak and is not shown. In the range 9.24 eV to the $3d^-$ ionization threshold at 10.79 eV we find resonances due to $3d^- \rightarrow np$ ($n > 5$) and $3d^- \rightarrow nf$ excitations which are degenerate in energy with $4s \rightarrow kp$ excitations. These resonances do not have a strong effect on the over-all shape of the spectrum and have not been shown in the figures. We calculated a strong resonance due to the $3d^+ \rightarrow 4p^+$ excitation which is degenerate with $4s^{\pm} \rightarrow kp$ excitations at $\omega = 12.132$ eV. Weaker resonances due to $3d^+ \rightarrow np^+$ excitations (for $n > 5$) are also indicated in Fig. 5. The height and shape of these resonances have not been carefully determined, and we have only indicated the approximate position of the resonances in Figs. 5 and 6. In Fig. 6 we do not show the resonances $3d^+ \rightarrow np^+$ for $n \geq 5$. There are also resonances for $3d^+ \rightarrow nf^+$ excitations but these have little effect on the over-all shape of $\sigma(\omega)$. The $3d^+ \rightarrow np^+$ resonances are associated with autoionizing states $(3d)^5\,(4s)^2np$ $^5P\,^5D$, and ^5F in which the $(3d)^5$ core couples to ^4P, ^4D, ^4F, or ^4G. The experimental results are not expected to show single strong lines as indicated in Fig. 5 and subsequent figures but should show much structure due to all the $(3d)^5\,(4s)^2np$ autoionizing lines which will be split. It is to be noted that our results in the vicinity of the resonances are very crude since they only include the lowest-order contributions. We have only shown resonances to $n = 8$, but the series continued to $n = \infty$ at 15.81 eV.

In Figs. 7 and 8 we show $\sigma(\omega)$ for the $(3d)^6$ subshell. Transitions $3d^{\pm} \rightarrow kp$, $kf^{\pm}$ are included, and we have averaged over M_L. There are resonances due to Fig. 2(b) with $p = 3d^-$, $q = 3d^+$, and $k' = np^+$, nf^+ ($n \geq 4$). The $3d^+ \rightarrow 4p^+$ excitation has a strong effect on $\sigma_{3d}(\omega)$ but the other resonances are of less importance. They have been indicated in Fig. 7 but not in Fig. 8. In Fig. 9 we have plotted cross sections for the $3p$, $3s$, $2p$, and $2s$ subshells. Correlations were not included, and so these results include only the diagrams of Fig. 1(a) [or

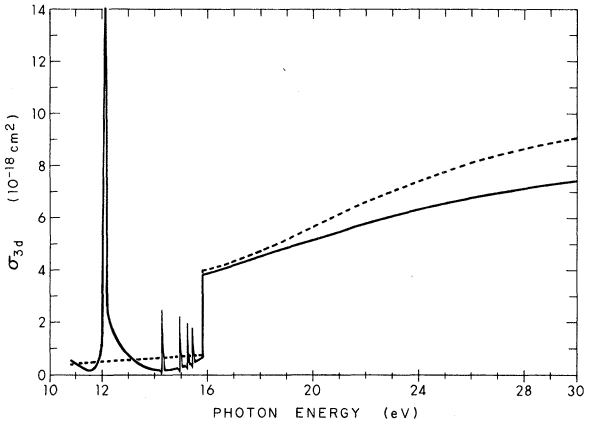

FIG. 7. Contribution to the photoionization cross section from the $(3d)^6$ subshell of Fe: Dashed line: Hartree-Fock or lowest-order result; solid line: includes correlations. Resonances shown are due to $(3d)^5(4s)^2\,np$ ^5P, ^5D, and ^5F autoionizing states. Our results near resonances are very approximate and also do not distinguish between different states for a given np. The height and shape of resonances have not been carefully calculated since we only included the lowest-order contribution to the resonances.

Fig. 2(a)].

The first threshold due to $4s^- \rightarrow kp^-$ excitations may be associated with the $(3d)^6\,4s\,^6D$ state of the ion. The next edge due to $4s^+ \rightarrow kp^+$ excitations is associated with the $(3d)^6\,4s\,^4D$ level of the ion. We note, however, that this association is not completely rigorous in this order of perturbation theory since the $(3d)^6\,^5D$ core with $M_S = +2$ and the remaining $4s^-$ electron give a mixture of ^6D and ^4D with relative probabilities $\frac{1}{5}$ and $\frac{4}{5}$.

The threshold due to ionization of the $3d^-$ electron is associated with the $(3d)^5\,(4s)^2\,^6S$ level of the ion. The second $3d$ threshold due to ionization of a $3d^+$ electron is associated with the $(3d)^5\,(4s)^2\,^4P$, ^4D, ^4F, and ^4G levels of the ion. As a result, in an experiment we expect to see more structure at this threshold than we have shown in our figures. We expect from spectroscopic data[17] and rough calculations that the splitting among these levels is approximately 1 eV. Again, there is also a small admixture of ^6S due to ionization of a $3d^+$ electron.

Our total Fe cross section is shown in Figs. 10 and 11. In addition to the resonance lines indicated, there are many additional resonances when we go to higher orders and include diagrams such as Figs. 3(a), 3(b), 3(d), and 3(e). The lowest-energy resonances involving these diagrams come from $(3d)^6\,(4s)^2\,^5D \rightarrow (3d)^6\,(mpns)\,^5F$, ^5D, ^5P excitations with $m \geq 4$ and $n \geq 5$, and from $(3d)^6\,(4s)^2\,^5D \rightarrow (3d)^6\,(mdnp)\,^5F$, ^5D, ^5P excitations with $m, n \geq 4$. We have calculated positions and widths for some of these levels, and results are listed in Table II.

However, we have not included these resonances in our calculated $\sigma(\omega)$; they may modify our $\sigma(\omega)$ when all diagrams of types shown in Fig. 3 are included as we plan to do in a future calculation. We note that our calculated excitations of Table II begin at $\omega = 9.424$ eV as compared with the $3d^+ \rightarrow 4p^+$ excitations at 12.132 eV. We expect that experiments on Fe will show many of these resonances.

IV. DISCUSSION AND CONCLUSIONS

This paper illustrates the use of many-body perturbation theory in calculating photoionization cross sections for complex atoms. The greatest surprise in the calculations is the large difference at threshold between the HF result for $\sigma(\omega)$ and the result including correlations. This is due to the relatively very large $\langle 4p \mid z \mid 4s \rangle$ matrix element which occurs in Fig. 2(b) with $p = 4s^{\pm}$, $q = 4s^{\mp}$, and $k' = 4p^{\mp}$. The oscillator strength for the $4s \rightarrow 4p$ excitation is so much larger than for $4s \rightarrow kp$ that the diagram of Fig. 2(b) contributes more to $\sigma(\omega)$ than the diagram of Fig. 2(a) near threshold. In terms of $\langle \Psi_K \mid \sum z_i \mid \Psi_i \rangle$, where Ψ_i is the exact initial state and Ψ_f is the exact final state, the diagram of Fig. 2(b) with $p = 4s^{\pm}$, $q = 4s^{\mp}$, and $k' = 4p$ corresponds to correlations in the state Ψ_K which mix configura-

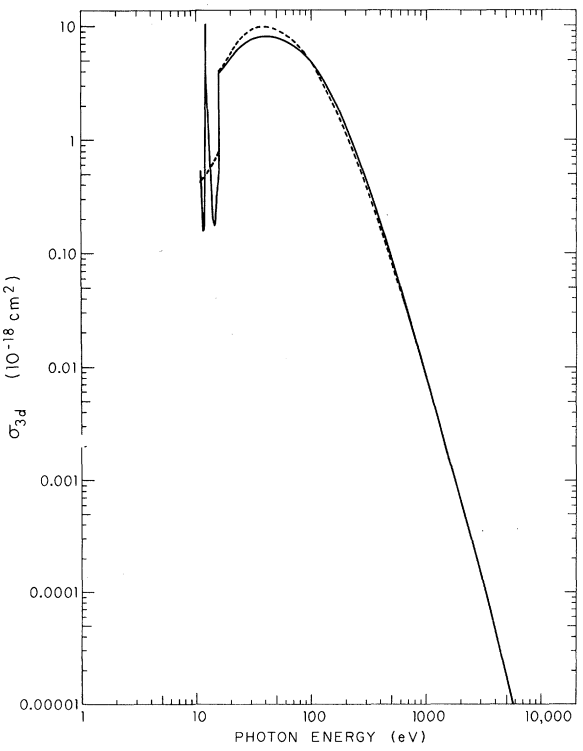

FIG. 8. Contribution to the photoionization cross section from the $(3d)^6$ subshell of Fe. Dashed line: Hartree-Fock or lowest-order result; solid line: includes correlations. More detail near threshold is given in Fig. 7.

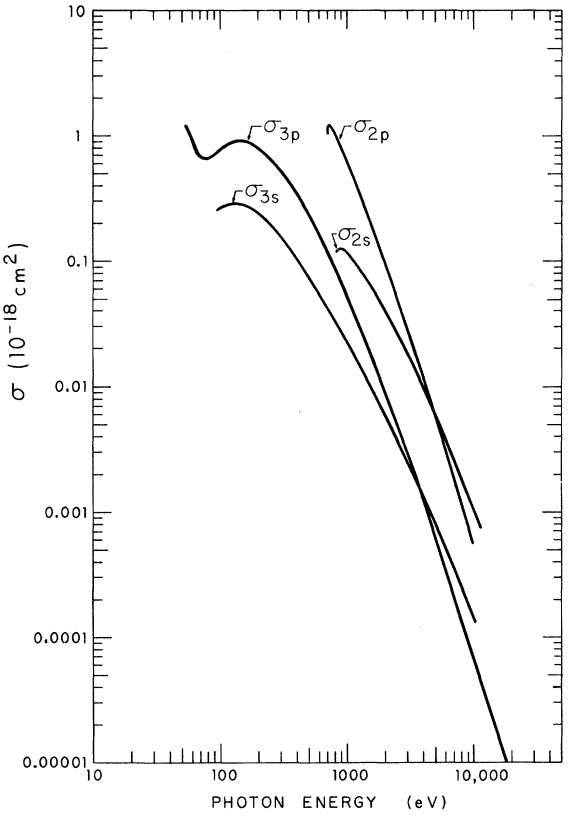

FIG. 9. Contributions to the photoionization cross section of Fe from the $(3p)^6$, $(3s)^2$, $(2p)^6$, and $(2s)^2$ subshells. These are our lowest-order results and do not include correlations. As described in the text, these results should be close to Hartree-Fock calculations.

tions $4p4s$ and $4skp$. The diagram of Fig. 2(d) with $p = 4s^{\pm}$, $q = 4s^{\mp}$, and $k' = 4p^{\mp}$ corresponds to correlations in Ψ_i which mix $(4s)^2$ with $(kp4p)$. We expect that such correlations in Ψ_K and Ψ_i play a very important role in photoionization cross sections for all atoms with an outer $(ns)^2$ subshell for $n \geq 2$.

In these calculations we included some effects of resonances and found a significant contribution from $3d^+ \rightarrow np^+$ excitations. We associate these resonances with autoionizing states $(3d)^5\,(4s)^2 np\,{}^5P$, ${}^5D$, and ${}^5F$, with a core $(3d)^5\,{}^4P$, ${}^4D$, ${}^4F$, or ${}^4G$. Our determinations of the detailed structure of the resonances is very inexact; and we plan in a future paper to calculate the resonance structure more accurately by going to higher orders in the perturbation expansion. We note that there are many resonances which we have not included in our final results and which may affect $\sigma(\omega)$, expecially near threshold. The most important of these are probably the $(4s)^2 \rightarrow (mpns)$ excitations with $m \geq 4$ and $n \geq 5$, and $(4s)^2 \rightarrow (md\,np)$ with $m, n \geq 4$. In this paper we have only fully included open diagrams of Fig. 2 with one interaction with H_c' and the $(4s)^2 \rightarrow (mpns)$ resonances occur in open diagrams with two or more interactions with H_c'. We plan to extend our calculations in a future paper and to include these contributions to $\sigma(\omega)$.

In calculating contributions to $\sigma(\omega)$ from the $3p$, $3s$, $2p$, $2s$, and $1s$ subshells, we have not included the effects of correlations, however, it would still be desirable to make a detailed calculation of correlation effects on $\sigma(\omega)$ from these subshells. Our contribution to $\sigma(\omega)$ from the $(3p)^6$ subshell near threshold is lower than that measured by Sonntag *et al.* for Fe metal.[21] The lack of agreement near threshold may be due to the metal environment and/or to electron correlations. In our curves for $\sigma(\omega)$ we give results from 0 eV to 10 keV, but the range of validity may be much less than 10 keV since we have omitted relativistic effects and have used the dipole approximation. However, our results are in good agreement with those of Rakavy and Ron[22] who calculated $\sigma(\omega)$ for Fe and other elements for $\omega = 1$–2000 keV using the Dirac equation with a modified Fermi-Amaldi potential. We plan in a future paper to investigate the combined effects of relativistic and many-body corrections.

Although it is very difficult to assess the accuracy of our results, we estimate our absorption coefficient near threshold, when integrated over a few eV, to be accurate to within approximately a

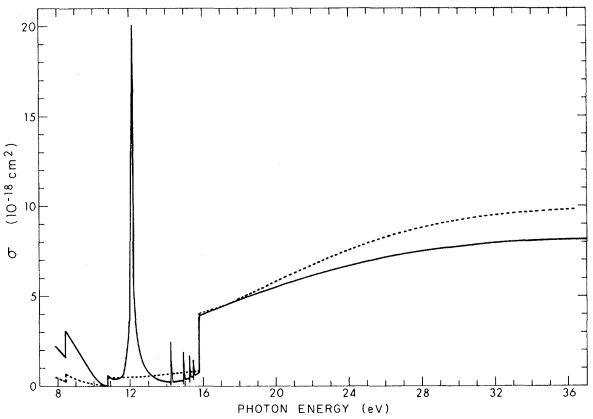

FIG. 10. Total photoionization cross section of Fe. Dashed line: lowest-order result (this is close to HF as described in text); solid line: includes correlations for contributions from $(4s)^2$ and $(3d)^6$ subshells. Resonances shown are due to autoionizing states $(3d)^5(4s)^2\,np\,{}^5P$, ${}^5D$, and ${}^5F$ with a $(3d)^5\,{}^4P$, ${}^4D$, ${}^4F$, or ${}^4G$ core. Contributions from all states with given np are shown as a single line. However, experiments should show splitting of these lines. Results in the vicinity of resonances have not been accurately determined and the shape of the resonances is very approximate. Also, as explained in the text, many resonances are not shown. Although we have only shown resonances to $n = 8$, the series continues to $n = \infty$ at 15.8 eV.

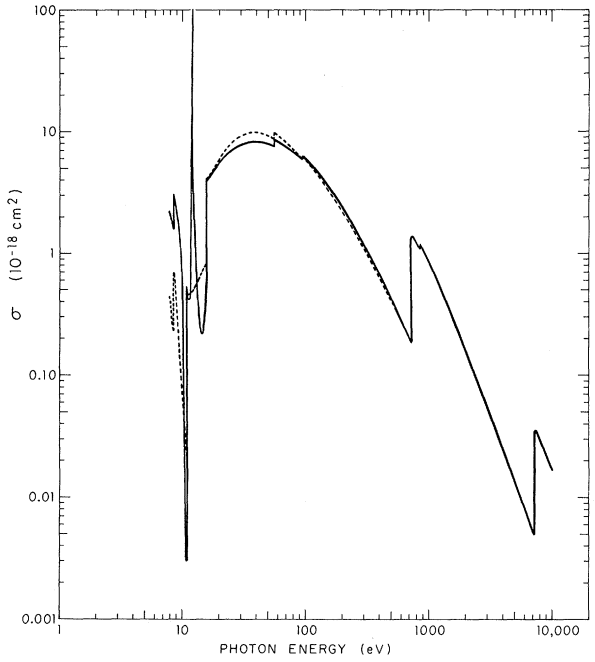

FIG. 11. Total photoionization cross section of Fe. Dashed line: lowest-order result (this result should be close to HF as described in text); solid line: includes correlations from $(4s)^2$ and $(3d)^6$ subshells. More detail near threshold is given in Fig. 10.

factor of 2. At higher energies our results should be more accurate.

Further contributions to the total cross section which we have not included are processes in which two or more electrons are ejected in the photo-

TABLE II. Some autoionizing levels contributing to diagrams of Fig. 3.

State	Energy above $(3d)^6(4s)^2\ ^5D$ (a.u.)[a]	Γ (a.u.)[a]
$(3d)^6\ ^5D(4p5s)\ ^1P\ ^5F$	0.3568	0.0207
^5D	0.3463	0.0223
^5P	0.3646	0.0200
$(3d)^6\ ^5D(4p6s)\ ^1P\ ^5F$	0.3967	0.0059
^5D	0.3861	0.0062
^5P	0.4045	0.0057
$(3d)^6\ ^5D(5p5s)\ ^1P\ ^5F$	0.5270	0.0015
^5D	0.5248	0.0016
^5P	0.5286	0.0015
$(3d)^6\ ^5D(4d4p)\ ^1P\ ^5F$	0.4000	0.00038
^5D	0.3991	0.00039
^5P	0.4008	0.00038

[a]Calculated values.

ionization. Another contribution which may also be important is the cross section for simultaneous photoionization and excitation of the resulting ion. We are presently calculating these cross sections.

Although the present calculations involved much effort, our final results may still be rather inaccurate; and there appears to be a need for continued experimental and calculational effort.

ACKNOWLEDGMENTS

We wish to thank Professor O. Gingerich for his comments which stimulated this work. We also are grateful to Professor J. W. Beams for his encouragement. We wish to thank Dr. R. L. Chase for the generous use of two of his computer programs.

*Research supported by the Aerospace Research Laboratories, Office of Aerospace Research, United States Air Force, Contract No. F 33615-69-C-1048.

†Permanent address: Department of Theoretical Physics, The Hebrew University, Jerusalem, Israel.

[1]U. Fano and J. W. Cooper, Rev. Mod. Phys. 40, 441 (1968).

[2]G. V. Marr, *Photoionization Processes in Gases* (Academic, New York, 1967).

[3]O. Gingerich (private communication).

[4]K. A. Brueckner, Phys. Rev. 97, 1353 (1955); *The Many-Body Problem* (Wiley, New York, 1959).

[5]J. Goldstone, Proc. Roy. Soc. (London) A239, 267 (1957).

[6]H. P. Kelly, Phys. Rev. 131, 684 (1963).

[7]H. P. Kelly, Phys. Rev. 136, B896 (1964).

[8]H. P. Kelly, Phys. Rev. 144, 39 (1966).

[9]E. S. Chang and M. R. C. McDowell, Phys. Rev. 176, 126 (1968).

[10]H. P. Kelly, in *Correlation Structure in Atoms* (Academic, New York, 1968), p. 75.

[11]H. P. Kelly, Phys. Rev. 182, 84 (1969).

[12]M. Ya. Amusia, J. Phys. B (to be published).

[13]M. Ya. Amusia, N. A. Cherepkov, and L. V. Chernysheva, Phys. Letters 31A, 553 (1970).

[14]G. Wendin, J. Phys. B 3, 455 (1970); 3, 466 (1970).

[15]H. A. Bethe and E. E. Salpeter, *Quantum Mechanics of One and Two-Electron Atoms* (Academic, New York, 1957), p. 306.

[16]H. Kelly and A. Ron, Phys. Rev. A 2, 1261 (1970).

[17]C. E. Moore, *Atomic Energy Levels*, Natl. Bur. Std. Cir. No. 467 (U. S. GPO, Washington, D. C., 1949).

[18]K. Siegban, C. Nordling, A. Fahlman, R. Nordberg, K. Hamrin, J. Hedman, G. Johansson, T. Bergmark, S.-V. Karlsson, I. Lindgren, and B. Lindberg, *ESCA Atomic, Molecular, and Solid State Structure Studied, by Means of Electron Spectroscopy* (Almqvist & Wiksells Boktryckeri AB, Uppsala, 1967).

[19]H. Kelly, Phys. Rev. A 1, 274 (1970).

[20]H. Kelly, and A. Ron, Phys. Rev. A 4, 11 (1971).

[21]B. Sonntag, R. Haensel, and C. Kunz, Solid State Commun. 7, 597 (1969).

[22]G. Rakavy and A. Ron, Phys. Rev. 159, 50 (1967).